Korean J. Chem. Eng., 34(11), 2811-2822 (2017)
DOI: 10.1007/s11814-017-0208-9

pISSN: 0256-1115
eISSN: 1975-7220

Computational fluid dynamics simulation of hydrodynamics in an uncovered unbaffled tank agitated by pitched blade turbines

Liangchao Li[*,†], **Jiajun Wang**[**], **Lianfang Feng**[**], **and Xueping Gu**[**]

*Key Laboratory of Testing Technology for Manufacturing Process of Ministry of Education,
School of Manufacturing Science and Engineering, Southwest University of Science and Technology,
Mianyang, Sichuan 621010, P. R. China
**State Key Laboratory of Chemical Engineering, College of Chemical and Biological Engineering,
Zhejiang University, Hangzhou 310027, P. R. China

(*Received 21 February 2017 • accepted 1 August 2017*)

Abstract−Computational fluid dynamics (CFD) simulations were applied for evaluating the hydrodynamics characteristics in an uncovered unbaffled tank agitated by pitched blade turbines. A volume of fluid (VOF) method along with a Reynolds stress model (RSM) was used to capture the gas-liquid interface and the turbulence flow in the tank. The reliability and accuracy of the simulations are verified. The simulation results show that the vortex can be divided into central zone and peripheral zone, and flow field in the tank can be divided into forced vortex flow region and free vortex flow region. With the increase of impeller speed, the vortex becomes deeper, while the critical radius of the two zones keeps almost unchanged. The impeller clearance and the rotational direction have little effect on the vortex shape. The vortex becomes deeper with increasing of the impeller diameter or the blade angles at the same rotational speed. Power number is little influenced by the impeller speed, and decreases by about 30% when impeller diameter varies from 0.25T to 0.5T. When blade angle varies from 30° to 90°, power number increases by about 2.32-times. Power number in uncovered unbaffled tank is much smaller than that in baffled tank, but is very close to that in a covered unbaffled tank. The discrepancy of power number in uncovered unbaffled tank and that in covered unbaffled tank is less than 10%.

Keywords: Uncovered Unbaffled Agitated Tank, Numerical Simulation, Computational Fluid Dynamics (CFD), Pitched Blade Turbine, Free Surface Vortex

INTRODUCTION

Most of the literature on mixing focused on baffled agitated tanks. Baffles in the tank can avoid the formation of vortex and enhance the mixing efficiency. However, just as some scholars pointed out [1-3], the presence of baffles can cause dead zones in the tanks. Besides, the presence of baffles may cause incrustation issues [4] or undesired precipitations [5], etc. In these cases, unbaffled tanks are a good alternative to overcome the shortcomings of baffled tanks. Furthermore, unbaffled tanks consume less power than baffled tanks [6]. The vortex in the liquid surface of unbaffled tank can be used in some processes, such as drawing down floating particles into the liquid, and removing gas bubbles from the liquid to reduce foam formation. For these advantages, uncovered unbaffled agitated tanks are applied in many industrial processes, such as crystallization, solid suspension, fermentation, and so on. So far, most of experimental and computational researches have been conducted about baffled agitated tanks, while only a very limited number of studies are about unbaffled agitated tanks. With the growing industrial interest and applications of unbaffled agitated tanks, further researches on the hydrodynamics in the tanks should be carried out.

Some scholars have experimentally studied the vortex behavior, flow pattern, power consumption and mixing efficiency in uncovered unbaffled agitated tanks. Rieger et al. [7], for example, experimentally measured the vortex depth in an unbaffled tank agitated by a Rushton turbine and developed a correlation to predict the vortex depth. Rao [8] modified the correlation developed by Rieger et al. [7] and Zlokarnik et al. [9], making the correlation suitable for impeller mounted near the liquid surface. Ciofalo [10] measured the free-surface profiles in an unbaffled tank agitated by a Rushton turbine. Markopoulos [11] reviewed the literature on the correlations for the prediction of vortex depth and presented a critical discussion on the basis of a theoretical analysis. As for the flow pattern, researchers [8,11-13] found that there are two regions in the unbaffled agitated tank. One region in the center of the tank formed forced vortex flow with angular velocity almost equal to that of impeller, and another in the peripheral of the tank formed free vortex flow with decreasing liquid velocity along the radial location. Haque et al. [14,15] measured the radial and tangential velocities at different locations in unbaffled tanks using laser Doppler velocimetry (LDV). Power consumption in unbaffled agitated tank is also an issue of serious concern. Scargiali et al. [16] studied the power consumption characteristics in an uncovered unbaffled agitated tank under nonaerated conditions (subcritical regime) and aerated con-

---

[†] To whom correspondence should be addressed.
E-mail: tchllc@126.com

ditions (supercritical regime), and proposed a novel overall correlation to predict the power number for the two regimes. Rao et al. [17,18] investigated the power characteristics of surface aerators with baffles and without baffles, and proposed a correlation of power consumption for unbaffled systems under aerated conditions. Assirelli et al. [19] found that the power number in unbaffled tank is 5.4-times less than that in baffled tank agitated by a modified Rushton turbine. Unbaffled tanks are often regarded as poor mixers compared to baffled tanks. However, Busciglio et al. [20] surprisingly found that, when free-surface vortex bottom approached the impeller plane, mixing efficiencies became practically identical to those of baffled tanks.

With the developments of high performance computers and computing technologies, the computational fluid dynamics (CFD) technique has been used widely as a powerful and useful simulation tool to investigate the turbulent flow characteristics in agitated tanks. Nevertheless, more CFD simulation studies are focused on the baffled tanks in the last two decades, the CFD simulations of turbulent flow in unbaffled agitated tank are scanty. In the literature, others, such as Ciofalo et al. [10], Haque et al. [14,15], Glover et al. [21] and Yang et al. [22], studied the flow fields in unbaffled tanks with CFD method. In these simulations, the volume of fluid (VOF) method is often used to track the gas-liquid interface. With regard to the turbulence models, researchers found that the k-ε turbulence model has the drawback of low accuracy in predicting turbulence quantities of the flow fields [22], while the Reynolds stress model (RSM) [14,15], large eddy simulation (LES) [23], detached eddy simulation (DES) [22] and shear-stress transport (SST) model [14,15] can improve the accuracy.

Through the previous experimental and simulation studies, we have a relatively deep understanding of the hydrodynamics in uncovered unbaffled tanks. However, as the previous researches reviewed, mainly the Rushton turbine (RT) is used in uncovered unbaffled agitated tanks. As we know, the Rushton turbine (RT) and pitched blade turbine (PBT) are two typical traditional impellers. Pitched blade turbines are also widely used in the process industries. Nevertheless, the researches on hydrodynamics in uncovered unbaffled tanks agitated by pitched blade turbines are few reported. Thus, we conducted numerical simulations to investigate the turbulent flow characteristics in an uncovered unbaffled tank agitated by PBT impellers. This work focuses on the effect of impeller speed as well as system configurations, such as impeller diameter, impeller clearance from the tank bottom and the blade angle on the shape of the vortex, power consumption and flow pattern.

SOLUTION DOMAIN AND GEOMETRICAL MODELING

1. Mixing System

A schematic diagram of the agitated tank is shown in Fig. 1. A flat-bottomed cylindrical tank with diameter of T=0.19 m was agitated by a pitched blade turbine (PBT). The liquid working medium is water (ρ_l=998 kg/m^3, μ_l=0.00103 Pa·s) with liquid level of H=T at initial moment. There is an air (ρ_g=1.225 kg/m^3, μ_g=1.79×10^{-5} Pa·s) zone in the tank above the liquid level with height of H_0= 0.11 m. The surface tension coefficient between the phase of air and water is set as 0.0732 N/m. The diameter of the PBT impeller ranges from T/4 to T/2, and the clearance of the impeller from the tank bottom ranges from T/3 to T/2. The blade angle varies from 30° to 90°. In the following sections, without specific mention, the down pumping PBT impeller with blade angle of 45° is used.

2. Geometrical Modeling and Grid Division

In accordance with the axial symmetry of the mixing system and the periodicity of the flow field in the tank, only one-quarter of the tank was simulated and two periodic boundaries were imposed along the azimuthal direction. A preprocessor Gambit 2.4 (Ansys Inc.) was used to generate the three-dimensional geometry and the computational mesh of the fluid domain. Fig. 2 shows the case

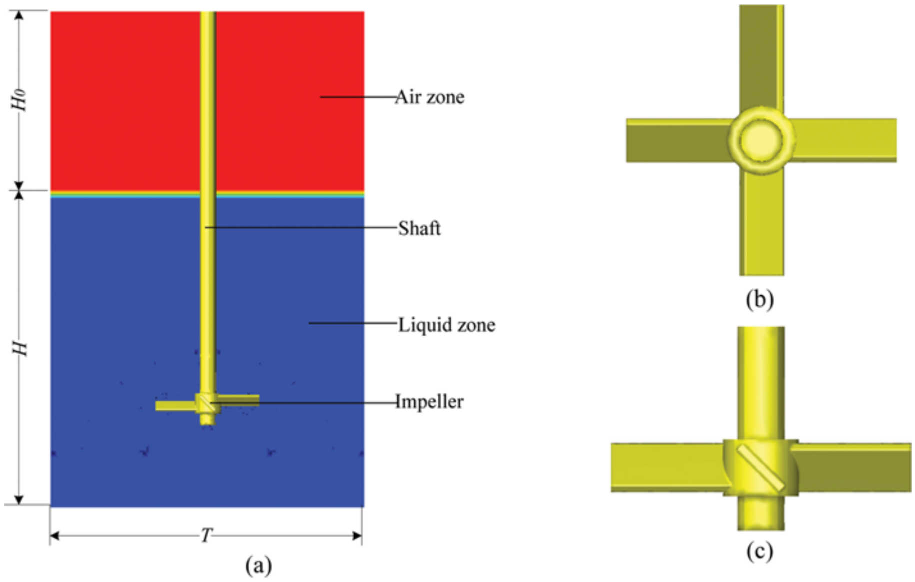

Fig. 1. Schematic diagram of the agitated tank and the pitch blade turbine for investigation: (a) agitated tank; (b) plan view of the impeller; (c) front view of the impeller.

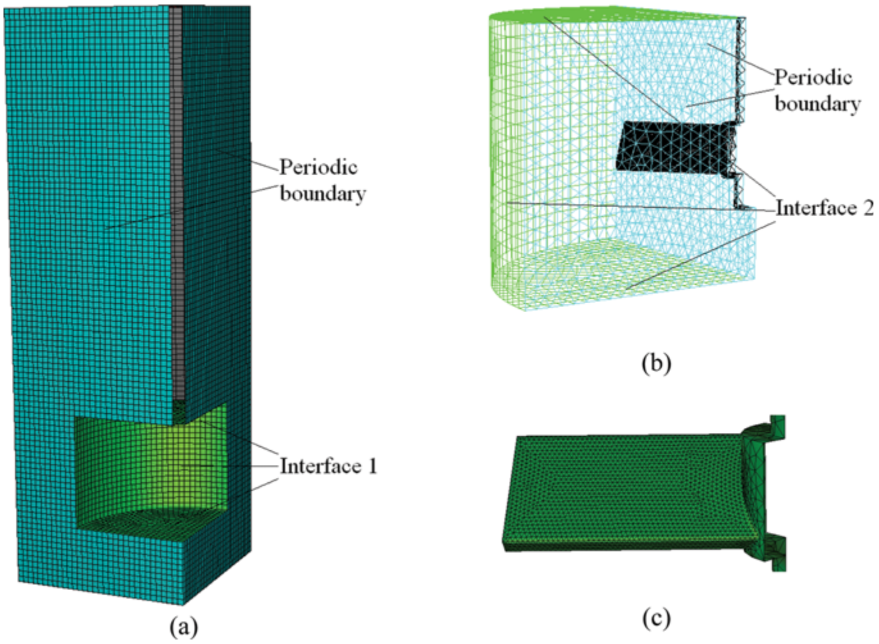

Fig. 2. Computational grid details of the agitated tank: (a) mesh for stationary region; (b) mesh for the impeller region; (c) refined mesh on the blade.

with C=T/3 and D=T/3. The fluid domain was divided into the impeller region and other stationary region to meet a multiple reference frame (MRF) approach to solve the rotation of the impeller. Grids were divided for the two regions, respectively. An adaptable tetrahedral mesh was used for the impeller region because of the complex structure of the PBT impeller, while a hexahedral mesh was employed for the stationary region to improve the convergence of the calculations and reduce the number of the grid elements. Furthermore, the mesh on the surface of the blades was refined to improve the accuracy of the simulation. The grid independency was tested by comparing the values of power number and free surface profile with different number of computational cells, and we found that the values obtained with chosen mesh and the finer mesh are almost the same. Finally, the total number of computational elements ranged from 170,000 to 240,000 for all of the investigated fluid domains.

MATHEMATICAL MODEL

1. Governing Equations

A homogeneous multiphase flow model coupled with a VOF method was used in the simulation to predict the flow field and the vortex shape in the unbaffled agitated tank. The general conversations of the continuity and momentum equations that solved throughout of the fluid domain were as follows:

$$\frac{\partial \rho_m}{\partial t}+\nabla\cdot(\rho_m U)=0 \tag{1}$$

$$\frac{\partial}{\partial t}(\rho_m U)+\nabla\cdot(\rho_m UU)=-\nabla p+\nabla\cdot[\mu_m(\nabla U+\nabla U^T)]+\rho_m g+F \tag{2}$$

where U is the resulting velocity, which is shared by both of the phases. p is static pressure. g is acceleration due to the gravity, and F is the body force. The μ_m and ρ_m are volume-weighted mixture's physical properties of viscosity and density, respectively.

2. VOF Model

The liquid-free surface is deformed under the stirring operating conditions. To determine the shape of liquid-free surface, a VOF method was used to capture the interface of air and water. The VOF model was solved in each cell that the volume fraction of the two or more interpenetrated phases is total to unity. The volume fraction of each phase can be obtained by solving a continuity equation. Furthermore, the properties and variables in each cell are the volume-weighted values of all the phases. The continuity equation and other relevant equations can be written as follows:

$$\frac{\partial \alpha}{\partial t}+U\cdot\nabla(\alpha)=0 \tag{3}$$

$$\alpha_g+\alpha_l=1.0 \tag{4}$$

$$\rho_m=\rho_l\alpha_l+\rho_g\alpha_g \tag{5}$$

$$\mu_m=\mu_l\alpha_l+\mu_g\alpha_g \tag{6}$$

The volume fraction of gas α_g will be 1.0 if the computational cell is in pure gas zones, and zero if the cell is in pure liquid zones. The gas-liquid interface can be determined by identifying the cells where the volume fraction of gas is $0<\alpha_g<1.0$.

3. Turbulence Model

In this work, the minimum impeller diameter D is T/4. Then, the minimum Reynolds number is 1.5×10^4 according to the definition of Reynolds numbers in agitated tanks as $Re=\rho_l ND^2/\mu_l$. It can be seen that the fluid flow in the tank is fully turbulent under all the operating conditions. The fluctuations of flow can be of small scale and high frequency, and are too computationally expensive

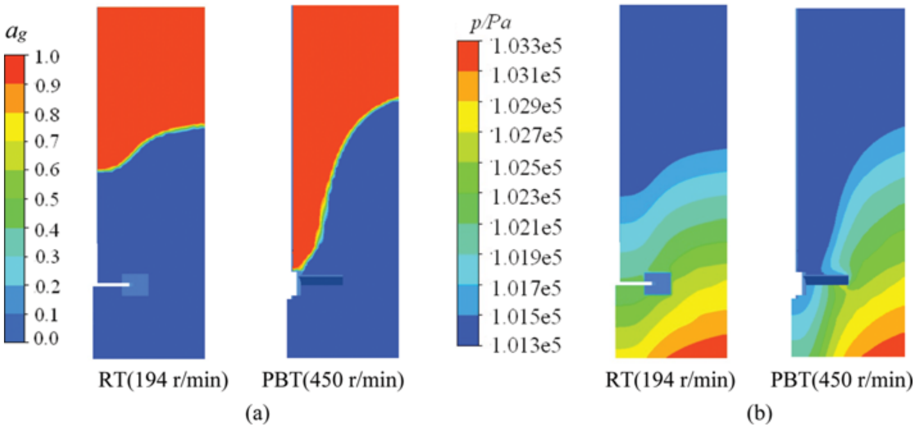

Fig. 3. The simulated absolute pressure and gas holdup distributions in the uncovered unbaffled tanks (C=T/3, D=T/2): (a) Gas holdup distribution; (b) absolute pressure distribution.

to simulate directly. As an alternative, the governing equations of the turbulent model can be modified by being time-averaged, ensemble-averaged, or otherwise manipulated to remove the small scales to reduce the computational cost. The modified equations known as Reynolds-averaged Naiver-Stokes (RANS) turbulent model include the closure models such as Spalart-Allmaras, *k-ε*, *k-ω* and Reynolds stress model (RSM). In these turbulence models, the RSM is one of the most accurate and used by many to describe the turbulent flow in the agitated tank. Different varieties of Reynolds stress model (RSM) are available, in which the version proposed by Speziale, Sarkar and Gatski (SSG) [24] is more accurate than the others. The SSG version of Reynolds stress model is used in the present work and its transport equations can be written as follows:

$$\frac{\partial(\rho_m\overline{u_iu_j})}{\partial t}+\frac{\partial(U_k\rho_m\overline{u_iu_j})}{\partial x_k}=\frac{\partial}{\partial x_k}\left[\left(\mu_m+\frac{2}{3}C_s\rho_m\frac{k^2}{\varepsilon}\right)\frac{\partial\overline{u_iu_j}}{\partial x_k}\right] \\ +P_{ij}-\frac{2}{3}\delta_{ij}\rho_m\varepsilon+\phi_{ij} \tag{7}$$

where P_{ij} is the exact production term, and is given by

$$P_{ij}=-\rho_m\overline{u_iu_k}\frac{\partial U_j}{\partial x_k}-\rho_m\overline{u_ju_k}\frac{\partial U_i}{\partial x_k} \tag{8}$$

where ϕ_{ij} is the pressure-strain correlation. The SSG model uses a quadratic relation for the pressure-strain correlation. For more details about the correlation, see the content in the literature [25].

In addition, the equation for turbulence dissipation ε that appears in the individual stress equations has the form as:

$$\frac{\partial(\rho_m\varepsilon)}{\partial t}+\frac{\partial(\rho_mU_k\varepsilon)}{\partial x_k}=\frac{\partial}{\partial x_k}\left[\left(\mu_m+\frac{\mu_t}{\sigma_\varepsilon}\right)\frac{\partial\varepsilon}{\partial x_k}\right]+\frac{\varepsilon}{\kappa}(C_{\varepsilon1}P_\kappa-C_{\varepsilon2}\rho_m\varepsilon) \tag{9}$$

4. Computation Details

Numerical simulations were conducted using a commercial CFD package CFX 10.0. The unsteady calculations were performed with time step of 0.01 s. At the initial moment, the impeller speed was zero, and the liquid was rest at the height of H=T. The impeller speed N ranged from 200 to 450 r/min for all the operating conditions. No slip boundary conditions were set for the tank bottom, sidewall, surface of blades and shaft, and the turbulent flow in these near-wall regions was treated with a scalable wall function. As mentioned, a multiple reference frame (MRF) method was used to treat rotation of the impeller. In this method, a moving reference frame with impeller rotational speed is set for the impeller region, while a stationary reference frame is applied for the stationary region. An opening type boundary condition was set for the top face of the tank with 0 Pa of gauge pressure. In the calculation, the convective terms in the model equations were discretized using the high-resolution scheme of the Ansys CFX, and the transient terms were discretized using a second implicit scheme. The discretization schemes were the same as that in the literature [26]. When the solution was final convergence, the total relative error was less than 1×10^{-4} for all the simulations.

RESULTS AND DISCUSSION

1. Model Validation

The reliability and accuracy of the simulation were verified in the tank agitated by Rushton turbine (RT) and pitched blade turbine (PBT), respectively. Fig. 3 shows the simulated gas holdup and absolute pressure distributions in the agitated tank. It can be seen

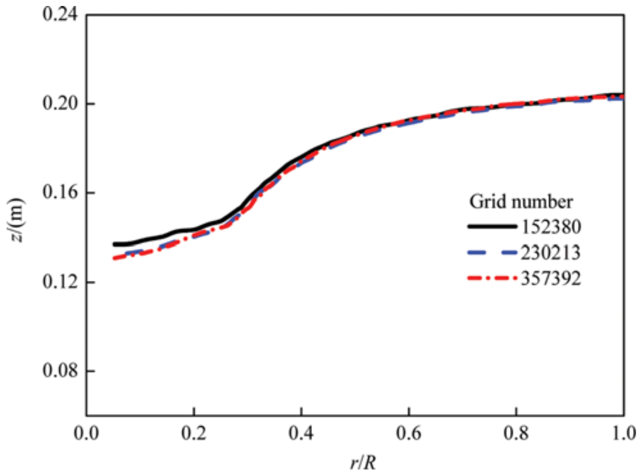

Fig. 4. Free surface profiles with different grid numbers (PBT impeller, C=T/3, D=T/2, N=300 r/min).

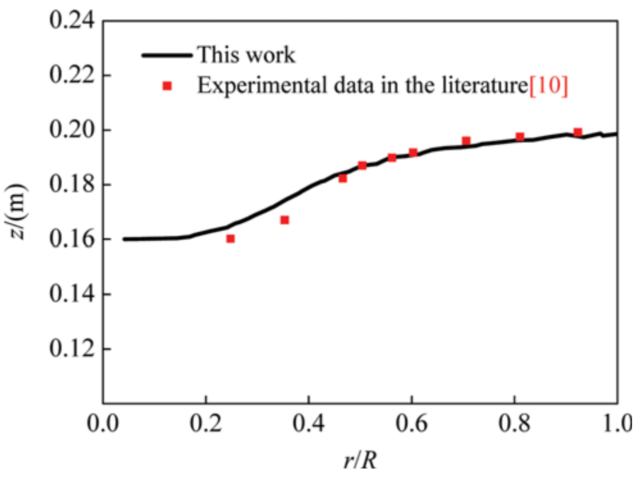

Fig. 5. Comparison of free surface profiles between simulated results and experimental data in the literature (RT, C=T/3, D=T/2, N=194 r/min).

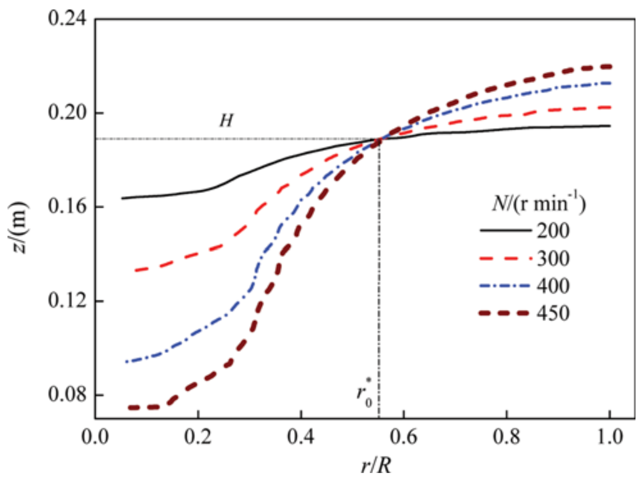

Fig. 7. Free surface profiles for different impeller speeds (PBT, C=T/3, D=T/2, β=45°).

that the vortex formed in the uncovered unbaffled tank. Under the effects of agitation and the variation of liquid free surface, the absolute pressure was deformed in the tank. The pressure in the center of tank was low and was the highest in the sidewall of the tank bottom. The grid number is very important for an accurate simulation. For the case with PBT impeller of D=T/2, three grid numbers, 152380, 230213, 357392 have been investigated. As shown in Fig. 4, the effect of grid number within the considered range on the free surface profile is small. Especially, the free surface profile with grid number of 230213 and that with 357392 is almost the same. Then, the grid number of 230213 was selected for this case. Furthermore, the simulated free surface profile in the tank agitated by Rushton turbine was compared with the experimental data in the literature [10] as shown in Fig. 5. Generally, the predicted vortex shape is consistent with that in the literature [10]. As shown in Fig. 3(a), the vortex bottom reaches to the horizontal plane of the PBT impeller, when the impeller speed is equal to 450 r/min. Tamburini [27] measured critical impeller speed for vortex bottom reaching to the location of impeller in a vortexing unbaffled agitated tank. For the same configuration (PBT, C=T/3, D=T/2, β=45°, T=0.19 m), the measured critical impeller speed was about 420 r/min. The experiment was in a solid-liquid tank. However, the solid loadings had no significant influence on the critical impeller speed (See Fig. 4 in the literature [27]). In addition, the predicted power number (N_p), vortex depth (h_v) are compared with the experimental results in the literature, which will be discussed in the following sections. Overall, the predicted hydrodynamics in this work is in good agreement with the experimental data in the literature.

2. Effect of Impeller Speed on Vortex Shape and Power Number

Fig. 6 shows the vortex shapes for different impeller rotational speeds. At the low impeller speed, the liquid level is relatively flat, and the vortex is shallow. With the increase of impeller speed, the centrifugal force increases, and the vortex becomes deeper. When the impeller speed is equal to 450 r/min, the vortex bottom reaches to the horizontal plane of the impeller.

For further study, the profiles of free surface for different impeller speeds are investigated as shown in Fig. 7. It can be seen that the vortex can be divided into two zones according to the liquid level (H=0.19 m) at the initial moment. The local liquid level falls

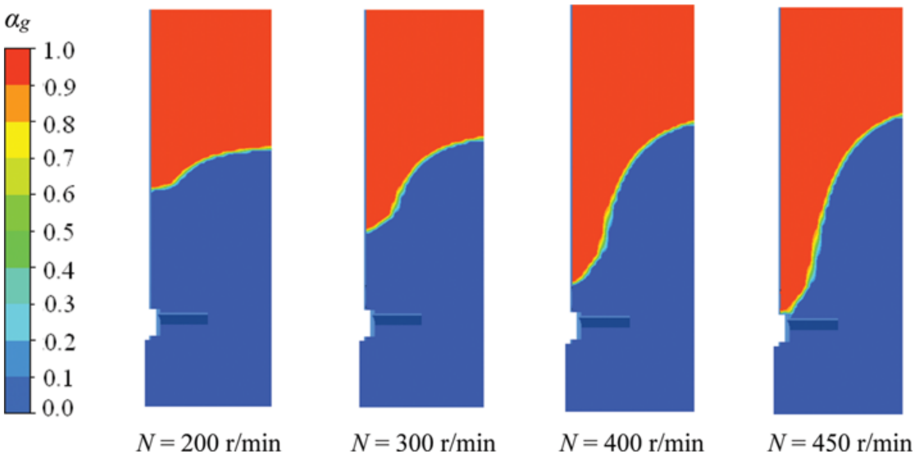

Fig. 6. Vortex shapes for different impeller speeds (PBT, C=T/3, D=T/2, β=45°).

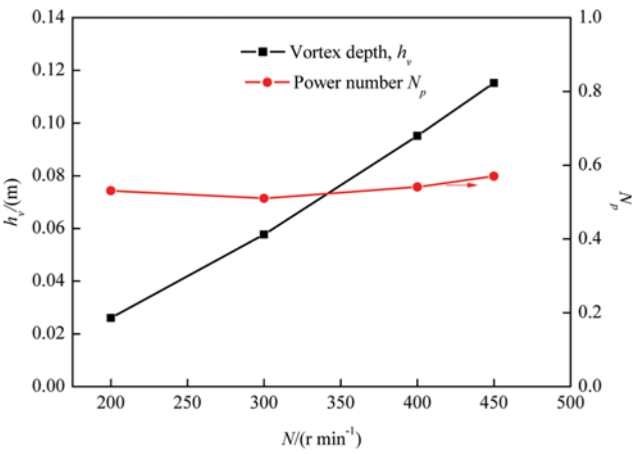

Fig. 8. Vortex depths and power numbers for different impeller speeds (PBT, C=T/3, D=T/2, β=45°).

for the central zone, while rises for the peripheral zone. Furthermore, for the same impeller, the nondimensional critical radial location, r_0^* of the two zones remains almost unchanged for different impeller speeds. The critical radius (r_0^*) on the liquid free surface is closely related to the flow pattern in the agitated tank. Rao et al. [8] experimentally studied the flow pattern in an uncovered unbaffled tank agitated by a disk turbine, and found that the critical radius of the forced vortex flow region and the free vortex flow region remains almost unchanged before the bottom of vortex reaches the impeller (See Fig. 2 in the literature [8]). It shows that the variation of critical radius with rotational speed for PBT impeller is similar to that of a disk turbine.

As shown in Fig. 8, the relationship between the vortex depth h_v and impeller speed N can be given as $h_v \propto N^{1.84}$. Researchers [8,28] determined the vortex depth is proportional to Froude number (Fr) for the rotational speed lower than the critical speed: $h_v \propto Fr = N^2D/g$. The fitted value, 1.84, in this work is close to that in the literature [8,28].

The power number N_p is an important parameter that reflects the agitation efficiency of the unbaffled tank, and can be calculated as:

$$N_P = \frac{P}{\rho_l N^3 D^5} \tag{10}$$

$$P = 2\pi MN \tag{11}$$

where P is power consumption, and M is the torque of the PBT impeller in the rotational direction, which can be obtained from the simulation results directly.

Fig. 8 gives the power number at different impeller speeds. The power number varies slightly with enhancing of the impeller speed and the averaged power number is 0.538. Scargiali et al. [29] investigated power number of different impellers in an uncovered unbaffled tank, and obtained the power number being almost constant until the free surface vortex reaches the impeller. Driss et al. [30] investigated PBT impeller power number in a covered unbaffled tank, and also determined that the power number remained constant in the turbulent flow range. Armenante et al. [31] measured the power number in a covered unbaffled agitated tank agitated by a PBT impeller. It was found that the power number changes from 0.670 to 0.617 when the impeller speed increases from 450 to 700 r/min. Furthermore, we evaluated the power number being about 0.45 for the same configuration in the literature [27] (See the experimental data in Fig. 4 in the literature [27]). In general, the power number predicted in this work is reliable and accurate.

3. Effect of Impeller Diameter on Vortex Shape and Power Number

The simulations were performed under the operating condition of the same impeller speed to study the effect of impeller diameter on the hydrodynamics in the uncovered unbaffled tank. As shown in Fig. 9, the vortex becomes larger and deeper with increasing of impeller diameter. It is attributed to the larger diameter causing higher centrifugal force in the tank. Fig. 10 shows the profiles of free surface for different impeller diameters. The critical radius r_0^* increases with increasing of the impeller diameters. By fitting the simulation data in the Fig. 11, at the same impeller speed, the vortex depth h_v and the impeller diameter D have the relation as $h_v \propto D^{2.4}$. Moreover, through analysis the correlation developed by Mar-

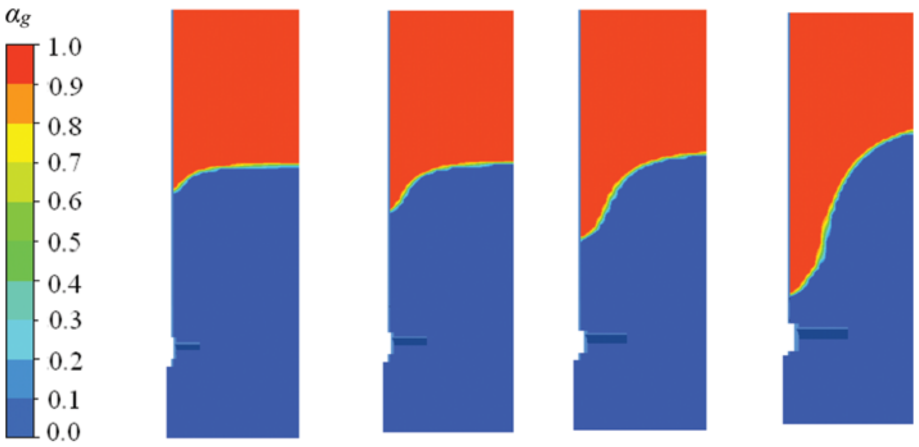

$D = T/4$ $D = T/3$ $D = 2T/5$ $D = T/2$

Fig. 9. Vortex shapes for different impeller diameters (C=T/3, N=400 r/min).

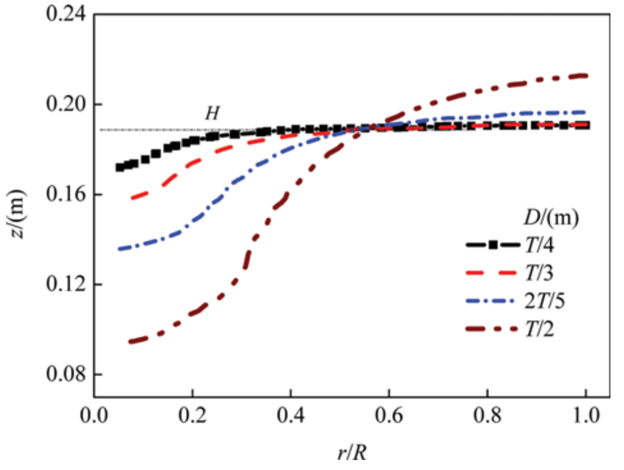

Fig. 10. Free surface profiles for different impeller diameters (C=T/3, N=400 r/min).

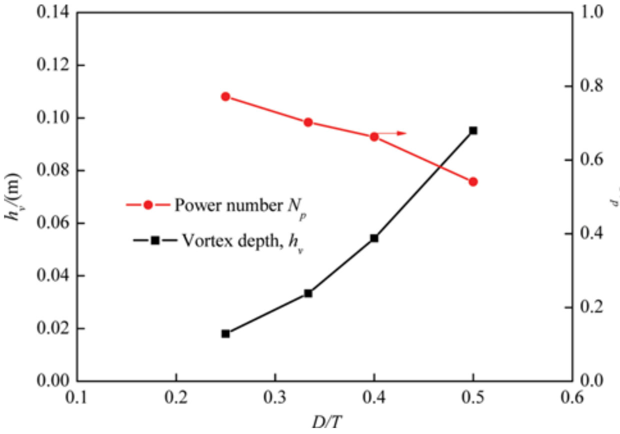

Fig. 11. Vortex depth and power numbers for different impeller diameters (C=T/3, N=400 r/min).

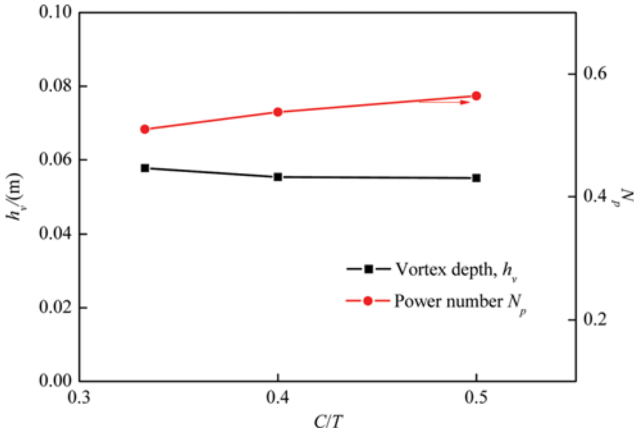

Fig. 13. Vortex depths and power numbers for different impeller clearances from tank bottom (D=T/2, N=300 r/min).

kopoulos et al. [28], the relationship between vortex depth and PBT impeller diameter is $h_v \propto D^{2.25}$, which is close to the simulation result in this work. Besides, larger impeller diameters result in smaller values of power number N_p. At the same impeller speed, the power number is decreased from 0.772 to 0.541 (See Fig. 11) when the impeller diameter varies from 0.25T to 0.5T. The power number decreases by about 30%. This finding is consistent with that in top-covered unbaffled tanks agitated by Rushton turbines [32]. In addition, Scargiali et al. [29] obtained through experimental measurement that power number decreases with increasing of impeller diameter before the vortex reaches the impeller, although they did not discuss this in their work.

4. Effect of Impeller Clearance from Tank Bottom on Vortex Shape and Power Number

Fig. 12 shows the vortex shapes with different impeller clearances from tank bottom. The vortex shape stays almost unchanged with the clearance. When the clearance varies from T/3 to T/2, the vortex depth h_v only decreases by 4.7% (See Fig. 13). It maybe can be interpreted by the velocity field in the tank. The vortex shape should be affected by the liquid velocity on the vortex. As shown in Fig. 12(b), the liquid velocity on the vortex is almost unchanged with the impeller clearance. Besides, we can find that the liquid velocity increases when radial location $r/R \le r_c^*$, but falls when radial

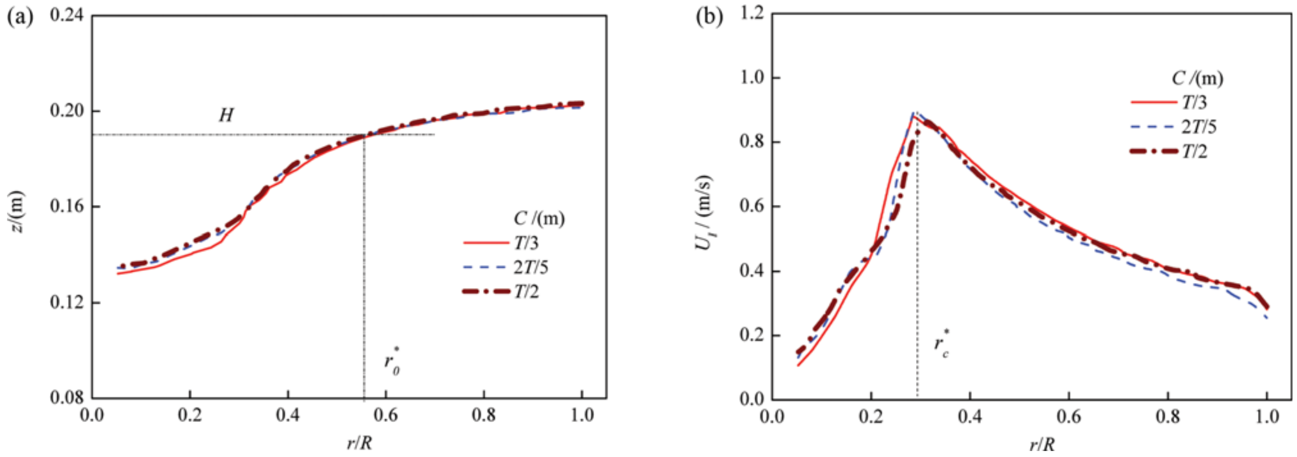

Fig. 12. Free surface profiles and liquid velocity on the free surface for different impeller clearances from tank bottom (D=T/2, N=300 r/min): (a) Free surface profiles; (b) mean velocity of liquid phase on the free surface.

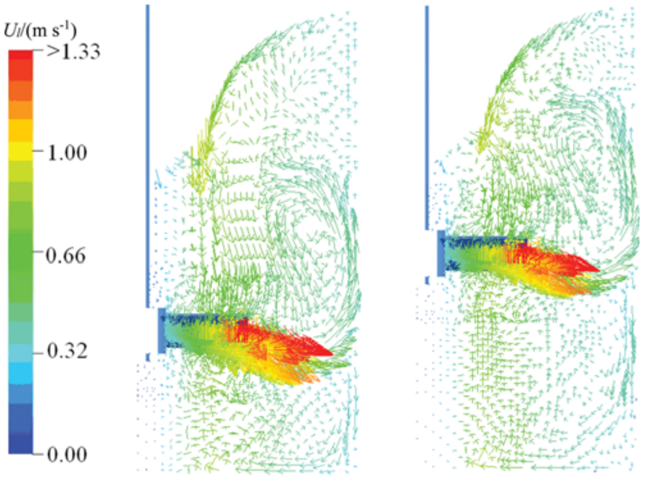

(a) (b)

Fig. 14. Flow patterns for different impeller clearances from tank bottom (D=T/2, N=300 r/min): (a) C=T/3; (b) C=T/2.

location $r/R \geq r_c^*$. For more details will be discussed in detail in the following section.

As shown in Fig. 13, the impeller power number N_p increases about 10.6% when the clearance rises from T/3 to T/2. In the literature, the effect of clearance on PBT impeller power number in uncovered unbaffled agitated tanks is rarely reported. However, some scholars investigated the PBT power number in baffled agitated tank. Bates et al. [33], for example, investigated the N_p in a baffled tank with PBT impeller, and found that the N_p increases when the clearance rises from T/3 to T/2. Nevertheless, Rewatkar et al. [34] reported that the N_p of PBT impellers in baffled tanks increases when the clearance falls from T/2 to T/6. They attributed it to the more dissipation of energy when the impeller is closer to the tank bottom. In addition, many [35-37] have found that the power number of a radial impeller increases with increasing of the clearance. The power number should be closely related to the flow pattern in the tank. As shown in Fig. 14, the axial flow is not obvious in the uncovered unbaffled tank agitated by PBT impeller. An indistinctive double-loop flow pattern is formed in the unbaffled tank agitated by PBT impeller, which is somewhat similar to the flow pattern generated by a radial impeller [35-37]. Consequently, the variation of power number with clearance would be also similar to that of radial impeller, i.e., power number rises with increasing of the clearance. In fact, the circumferential flow is dominant in the uncovered unbaffled tank. In the literature [12,38], some of the works dealing with unbaffled tank modeling also indicated that the axial variation of tangential velocity is small, with exception of the region adjacent to the tank bottom. It shows that the tangential velocity does not decay significantly along the axial height in the unbaffled tank, and the variation of clearance has no significant influence on the liquid velocity field. Thus, as a whole, the clearance has no great influence on the vortex depth and power number in high turbulent regime in uncovered unbaffled tank.

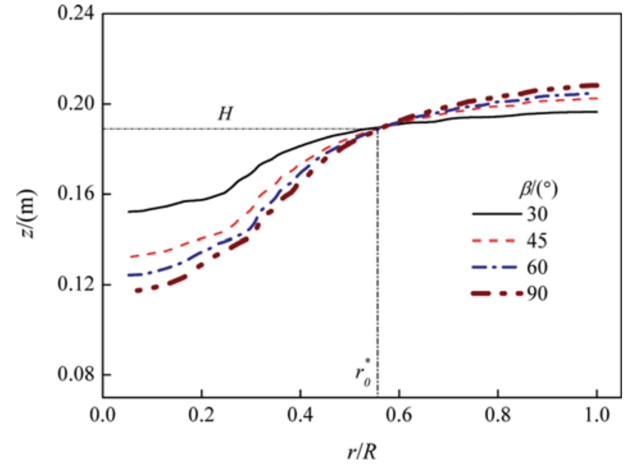

Fig. 15. Free surface profiles for different impeller blade angles (C=T/3, D=T/2, N=300 r/min).

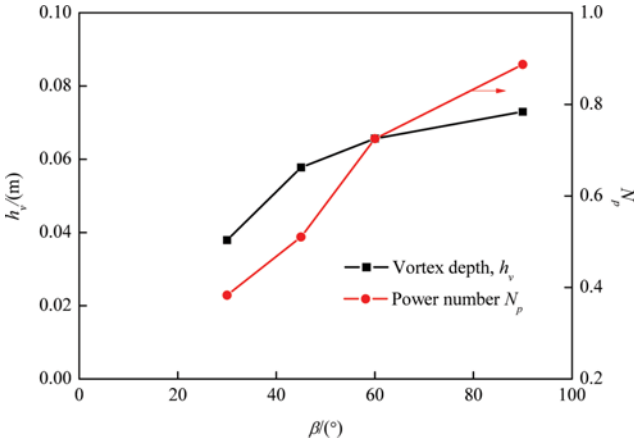

Fig. 16. Vortex depths and power numbers for different impeller angles (C=T/3, D=T/2, N=300 r/min).

5. Effect of Blade Angle on Vortex Shape and Power Number

The impeller blade angle β is the angle between the plane of blade and the horizontal axis. In this work, the blade angle β from 30° to 90° was investigated. The PBT impeller having the angle of 90° is actually a straight bladed turbine. In Fig. 15 and 16 the vortex becomes deeper with increasing of the blade angle, while the critical radius r_0^* stays constant. Besides, the blade angle has a strong effect on the PBT impeller power number N_p (See Fig. 16). When the blade angle varies from 30° to 90°, the power number increases by about 2.32 times. In the literature, Driss et al. [30] experimentally and CFD studied the power number for PBT impellers with three blade angles in a covered unbaffled tank, and also found that power number increases with increasing of the blade angle. In addition, Rewatkar et al. [34] found that power number increases with increasing of blade angle in a baffled tank. It maybe can be interpreted from the projected area of the impeller blade in the vertical direction. With the increase of the blade angle, the projected area becomes larger, and more fluid is discharged by the blade, which results in higher torque. As a result, power consumption and power number N_p increase.

6. Comparison of Vortex Shape and Power Number for Up and Down Pumping Impellers

The up or down pumping PBT impeller can be achieved by

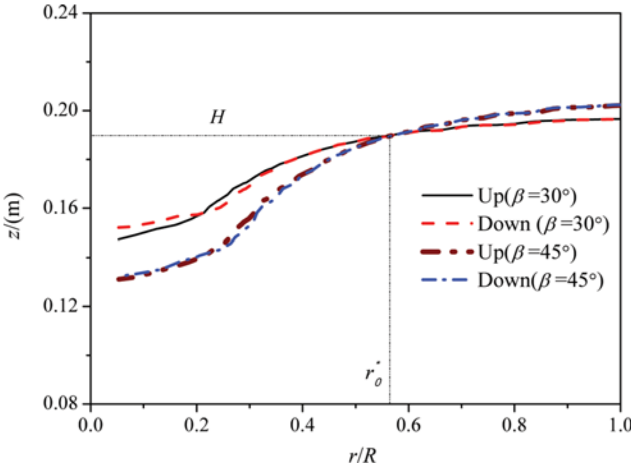

Fig. 17. Free surface profiles for up and down pumping impellers (C=T/3, D=T/2, N=300 r/min).

Table 1. Power number for up and down pumping impellers (C=T/3, D=T/2, N=300 r/min)

Blade angle β	Rotational direction	Power number N_p
30°	Up	0.377
	Down	0.383
45°	Up	0.554
	Down	0.510

changing the rotational direction. As shown in Fig. 17, the vortex shapes generated by up and down pumping impellers with angles of β=30° and 45° were investigated, respectively. The up and down pumping impellers have almost the same free surface profiles. As mentioned, the circumferential flow is dominant in the unbaffled tank. Furthermore, the circumferential flow should mainly be controlled by the blades' horizontal projected area. As a result, the rotational direction has little effect on the vortex shape. Table 1 lists the power number of the two impellers with different rotational directions. Generally, the rotational direction of the PBT impeller also has no significant effect on the power number in the uncovered unbaffled agitated tank.

7. Comparison of Flow Field with Baffled Tank and Covered Unbaffled Tank

Four baffles with width of T/10 were mounted equally in the unbaffled tank to form the baffled agitated tank. Since the liquid level is hardly deformed under stirring conditions in the baffled tank, the free surface is considered as horizontal free-slip wall, and only one single-phase is modeled in this simulation. The liquid velocities in a vertical plane (midway of two adjacent baffles for baffled tank) and in a horizontal plane (z=0.005 m) were investigated. As shown in Fig. 18, the flow fields in the two tanks are very different. As for the uncovered unbaffled tank, an indistinctive double-loop flow pattern is formed, which is similar to the flow pattern generated by radial impeller in baffled tanks. The axial flow is not obvious, and the circumferential flow is, in fact, dominant in the unbaffled tank. The liquid velocity in the near-bottom region increases firstly and then decreases along the radial direction. Different from that in unbaffled tank, one single-loop main flow pattern is formed in the baffled tank, and a secondary flow is formed just below the PBT impeller and in the near-surface region, respec-

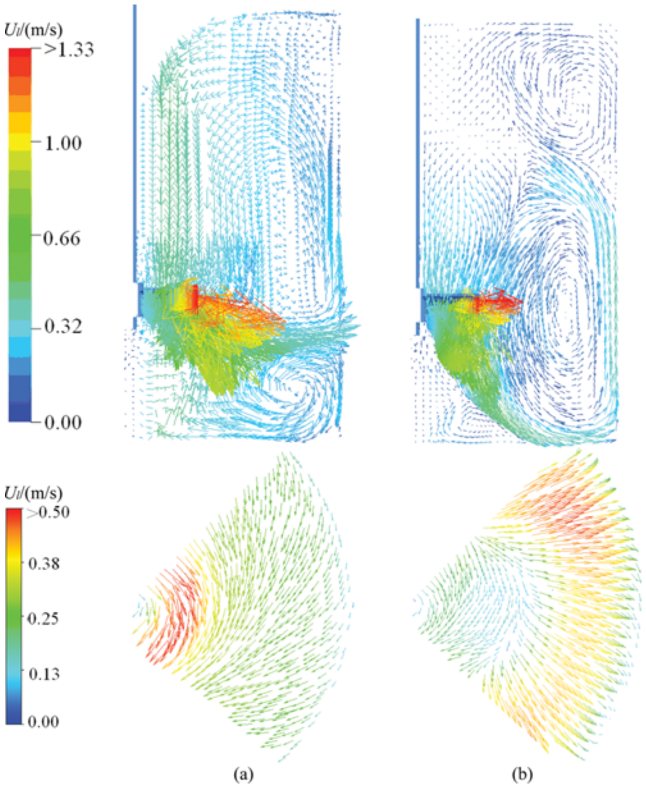

(a) (b)

Fig. 18. Velocity vector in different planes for unbaffled and baffled agitated tanks (C=T/3, D=T/3, N=400 r/min): (a) Unbaffled agitated tank; (b) baffled agitated tank.

Table 2. Comparison of power number for unbaffled and baffled agitated tanks

No.	H/T	C/T	D/T	n_b	w_b/T	N/(r/min)	N_p	Refs.
1	1.0	0.33	0.33	4	0	400	0.702	This work 1
2	1.0	0.33	0.33	4	0.1	400	1.28	This work 2
3	1.0	0.33	0.33	4	0	--	0.55	Scargiali et al. [29]
4	1.0	0.33	0.33	6	0	450	0.67	Armenante et al. [31]
5	1.0	0.33	0.42	4	0.1	150	1.27	Ge et al. [39]
6	1.0	0.33	0.33	4	0.1	--	1.24	Chapple et al. [40]
7	1.0	0.33	0.33	6	0.1	300	1.44-1.62	Moštěk et al. [41]

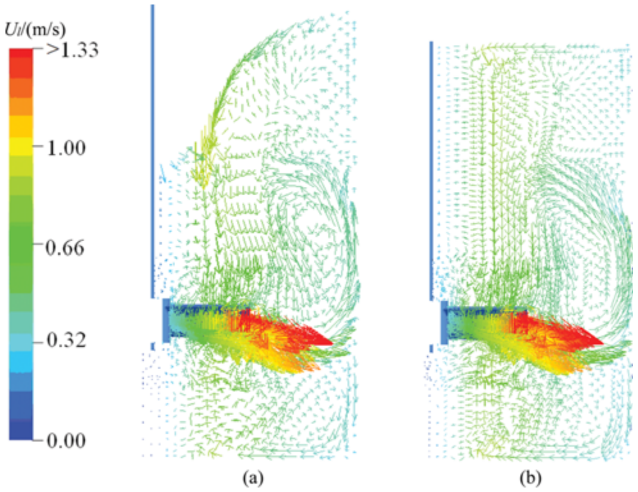

Fig. 19. Velocity vectors in vertical plane for covered and uncovered agitated tanks (C=T/3, D=T/2, N=300 r/min): (a) Uncovered agitated tank; (b) covered agitated tank.

tively. Furthermore, the radial flow is dominant in the near-bottom region, and the liquid velocity is relatively low in the center of the region.

Table 2 lists the power numbers of PBT impellers in the two tanks. The power number in the baffled tank is much higher than that in unbaffled tank. Scargiali et al. [29] obtained the PBT power number in an uncovered unbaffled tank being about 0.55 before the vortex reaches the impeller. Armenante et al. [31] experimentally measured the PBT power number N_p of 0.67 in a covered unbaffled tank. As for the PBT power number in baffled tank, Ge et al. [39] predicted that the PBT power number is 1.27 through CFD simulation. Chapple et al. [40] experimentally measured the PBT power number being about 1.24 for the impeller with diameter of D=T/3, when Reynolds number is $Re>2\times10^4$. Moštěk et al. [41] obtained the power number N_p=1.44-1.62 in a baffled tank agitated by a PBT impeller with six blades. Generally, the predicted power number of PBT impeller in this work is in good agreement with that in the literature [29,31,39-41].

As shown in Fig. 19, the flow pattern in covered unbaffled agitated tank is very similar to that in uncovered unbaffled tank. Both the tanks formed an indistinctive double-loop flow pattern. Furthermore, the structure and size of circulation loops for the two tanks are very close. Armenante et al. [31] and Kuncewicz et al. [42] also obtained similar results of flow pattern in covered unbaffled tank agitated by PBT impeller. The main difference for the two tanks was found in the near surface region. For the uncovered tank, the direction of liquid velocity on the vortex is parallel to the liquid free surface. However, the direction of the liquid velocity is horizontal in the near-surface region for the covered agitated tank. For the configuration of C=T/3, D=T/2 and N=300 r/min, the predicted power number N_p in uncovered and covered tank is 0.51 and 0.48, respectively. The discrepancy is about 5.9%. Recently, Scargiali et al. [43] experimentally studied the power number N_p in covered and uncovered tank agitated by a Rushton turbine. They found that the power number N_p in covered tank is very close to that in uncovered tank for Re<1000, while slightly larger for

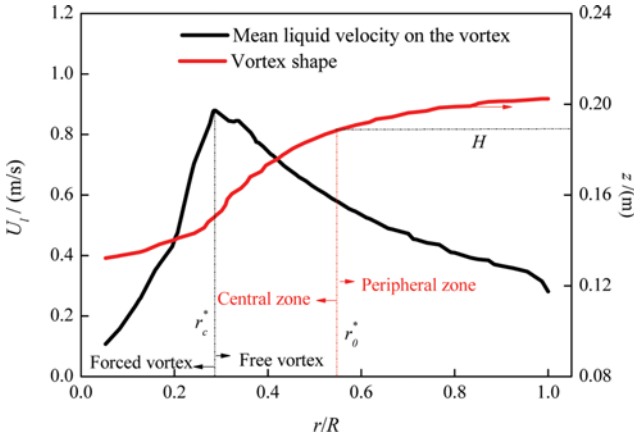

Fig. 20. Vortex shape and radial distribution of liquid velocity on the vortex (C=T/3, D=T/2, N=300 r/min).

Re>1000 (The discrepancy is smaller than 10%). In general, it can be seen that the top-cover has no significant effect on the power number N_p.

8. Forced Vortex and Free Vortex in the Unbaffled Agitated Tank

In the previous section, we found that liquid velocity on the vortex rises firstly and then decreases in the uncovered unbaffled tank. In fact, the flow field in the uncovered unbaffled tank can be divided into forced vortex flow region and free vortex flow region. Fig. 20 shows the vortex shape and liquid velocity distributions on the vortex. The liquid velocity almost increases linearly up in the forced vortex flow region ($r/R\le r_c^*$), while decreases slowly in the free vortex flow region ($r/R\ge r_c^*$). For the configuration of C=T/3, D=T/2 and N=300 r/min, the predicted critical radius r_c^* is about 0.28. The predicted result is close to those calculated values using correlations of Nagata [12] and Le Lan and Angelino [44].

$$\text{Nagata: } \frac{2r_c}{D}=\frac{Re}{2.11Re-15850} \tag{12}$$

$$\text{Le Lan: } \frac{2r_c}{D}=\frac{Re}{2.27Re-20630} \tag{13}$$

The calculated r_c^* using Nagata [12] and Le Lan and Angelino [44] models are 0.284 and 0.276, respectively. However, the correlations of Nagata [12] and Le Lan and Angelino [44] would not be accurate, or even in error for very low Reynolds number. For example, in this work, the minimum impeller diameter D is T/4. If the impeller speed is 200 r/min, the Reynolds number Re will be less than 7.5×10^3, and the calculated critical radius will be a negative value using the correlation of Nagata [12] or the correlation of Le Lan and Angelino [44]. It is unreasonable. Furthermore, note that the critical radius of the two types of vortex region r_c^* is different from the critical radius of two zones r_0^*. As discussed earlier, the latter is divided according to the variations of the local liquid level under stirring operating condition.

Table 3 lists the r_0^* and r_c^* under different operating conditions. The value of r_0^* is about 1.8-3.2-times than that of r_c^*. The variation of r_c^* with operating condition is almost in accordance with that of

Table 3. r_0^* and r_c^* under different operating conditions

D (m)	N (r/min)	C (m)	β (°)	Direction	r_0^*	r_c^*
T/2	200	T/3	45	Down	0.56	0.28
T/2	300	T/3	45	Down	0.56	0.28
T/2	400	T/3	45	Down	0.56	0.28
T/2	450	T/3	45	Down	0.56	0.28
T/2	300	2T/5	45	Down	0.56	0.29
T/2	300	T/2	45	Down	0.56	0.30
T/4	400	T/3	45	Down	0.46	0.14
T/3	400	T/3	45	Down	0.49	0.17
2T/5	400	T/3	45	Down	0.54	0.22
T/2	300	T/3	30	Down	0.55	0.28
T/2	300	T/3	60	Down	0.56	0.29
T/2	300	T/3	90	Down	0.56	0.31
T/2	300	T/3	30	Up	0.55	0.24
T/2	300	T/3	45	Up	0.56	0.28

r_0^*. The impeller speed, impeller clearance, blade angle and rotation direction have no significant effects on the r_0^* and r_c^*. Nevertheless, the r_0^* and r_c^* increase for larger impeller diameter.

CONCLUSIONS

Numerical predictions of the hydrodynamics characteristics in an uncovered unbaffled tank agitated by PBT impellers were performed by using a VOF method in conjunction with a Reynolds stress model (RSM). The modeling was validated by comparing the simulated results with experimental data in the literature. The main conclusions are as follows.

The vortex in the uncovered unbaffled agitated tank can be divided into central zone and peripheral zone according to the variation of the local liquid level. According to the velocity field distribution, the flow field in the tank can be divided into forced vortex flow region and free vortex flow region. The non-dimensional critical radius of two zones r_0^* is about 1.8-3.2-times than the non-dimensional critical radius of two regions r_c^*.

With enhancing of the impeller speed, the vortex becomes deeper, while the critical radius of the two zones r_0^* remains almost unchanged, and corresponding power number changes slightly. Impeller clearances from the tank bottom and the rotational direction have no significant influences on the vortex shape.

At the same impeller speed, the vortex becomes deeper and larger, and the non-dimensional critical radius of the two zones r_0^* increases with increasing of the impeller diameter, while the power number falls sharply. With increasing of the blade angle, the vortex becomes deeper, and the power number becomes higher. Power number in the uncovered unbaffled agitated tank is far lower than that in the corresponding baffled tank, while is close to that in the covered unbaffled tank.

ACKNOWLEDGEMENTS

The authors would like to acknowledge the support by Key Scientific Research Project of Sichuan Provincial Education Department (15ZA0107), National Key Research and Development Project of China (2016YFC1100801), State Key Laboratory of Chemical Engineering (SKL-Che-16D02) and the Fundamental Research Funds for the Central Universities.

NOMENCLATURE

C : impeller clearance from tank bottom [m]
C_s : model constant in Eq. (7) [-]
$C_{\varepsilon1}$, $C_{\varepsilon2}$: model constant in Eq. (9) [-]
D : impeller diameter [m]
F : body force, [N/m^3]
Fr : Froude number [-]
h_v : vortex depth [m]
H : liquid level [m]
H_0 : height of the air zone [m]
k : turbulent kinetic energy [m^2/s^2]
M : torque of the impeller in rotational direction [N m]
n_b : number of the blades [-]
N : impeller speed [r/min]
N_p : power number [-]
p : static pressure [Pa s]
P : power consumption [W]
P_{ij} : exact production term in Eq. (7) [kg/m s^3]
P_κ : production rate of turbulent kinetic energy [kg/m s^3]
r : radial location [m]
r_c : critical radius of the forced vortex and free vortex [-]
r_0^* : non-dimensional critical radius of the two zones of vortex [-]
r_c^* : non-dimensional critical radius of the forced vortex and free vortex [-]
R : tank radius [m]
Re : Reynolds number [-]
t : flow time [s]
T : tank diameter [m]
u_i, u_j : Reynolds stresses components [m/s]
U : fluid velocity vector [m/s]
w_b : width of the baffle [m]
z : axial height in the tank [m]

Greek Letters

α : phase volume fraction [-]
β : blade angle [°]
δ_{ij} : Kronecker delta [-]
ε : turbulence dissipation rate [m^2/s^3]
μ : viscosity [kg/m s]
μ_t : turbulent viscosity [kg/m s]
ρ : density [kg/m^3]
σ_ε : constant in Eq. (9) [-]
ϕ_{ij} : pressure-strain correlation [kg/m s^3]

Subscript

g : gas phase
i, j, k : coordinate system
l : liquid phase
t : turbulent

REFERENCES

1. D. J. Lamberto, F. J. Muzzil, P. D. Swanson and A. L. Tonkovich, *Chem. Eng. Sci.*, **51**, 733 (1996).
2. M. M. Álvarez, P. E. Arratia and F. J. Muzzio, *Can. J. Chem. Eng.*, **80**, 546 (2002).
3. Y. Y. Hu, Z. Liu, J. C Yang and Y. Cheng, *Chinese J. Chem. Eng.*, **61**, 2517 (2010).
4. J. M. Rousseaux, H. Muhr and E. Plasari, *Can. J. Chem. Eng.*, **79**, 697 (2001).
5. D. Hekmat, D. Hebel, H. Schmid and D. Weuster-Botz, *Process Biochem.*, **42**, 1649 (2007).
6. A. R. Rao and B. Kumar, *J. Chem. Technol. Biotechnol.*, **82**, 101 (2007).
7. F. Rieger, P. Ditl and V. Noval, *Chem. Eng. Sci.*, **34**, 397 (1979).
8. A. R. Rao, B. Kumar and A. K. Patel, *Science Asia*, **35**, 183 (2009).
9. M. Zlokarnik, *Chem. Eng. Technol.*, **43**, 1028 (1971).
10. M. Ciofalo, A. Brucato, F. Grisafi and N. Torraca, *Chem. Eng. Sci.*, **51**, 3357 (1996).
11. J. Markopoulos and E. Kontogeorgaki, *Chem. Eng. Technol.*, **18**, 68 (1995).
12. S. Nagata, *Mixing: Principles and Applications*, Wiley, New York (1975).
13. F. Grisafi, A. Brucato and L. Rizzuti, *Inst. Chem. Eng. Symp. Ser.*, **136**, 571 (1994).
14. J. N. Haque, T. Mahmud and K. J. Roberts, *Ind. Eng. Chem. Res.*, **45**, 2881 (2006).
15. J. N. Haque, T. Mahmud, K. J. Roberts, J. K. Liang, G. White, D. Wilkinson and D. Rhodes, *Can. J. Chem. Eng.*, **89**, 745 (2011).
16. F. Scargiali, A. Busciglio, F. Grisafi, A. Tamburini, G. Micale and A. Brucato, *Ind. Eng. Chem. Res.*, **52**, 14998 (2013).
17. A. R. Rao, A. Kumar Patel and B. Kumar, *J. Chem. Technol. Biotechnol.*, **85**, 805 (2010).
18. A. R. Rao and B. Kumar, *J. Hydraul. Div., Am. Soc. Civ. Eng.*, **135**, 38 (2009).
19. M. Assirelli, W. Bujalski, E. Archie and A. W. Nienow, *Chem. Eng. Sci.*, **63**, 35 (2008).
20. A. Busciglio, F. Grisafi, F. Scargiali and A. Brucato, *Chem. Eng. J.*, **254**, 201 (2014).
21. G. M. C. Glover and J. J. Fitzpatrick, *Chem. Eng. J.*, **127**, 11 (2007).
22. F. L. Yang and S. J. Zhou, *Chem. Biochem. Eng. Q.*, **29**, 395 (2015).
23. N. Lamarque, B. Zoppé, Q. Lebaigue, Y. Dolias, M. Bertrand and F. Ducros, *Chem. Eng. Sci.*, **65**, 4307 (2010).
24. C. G. Speziale, S. Sarkar and T. B. Gatski, *J. Fluid Mech.*, **277**, 245 (1991).
25. F. Nemdili, A. Azzi, G. Theodoridis and B. A. Jubran, *Heat Transfer. Eng.*, **11**, 950 (2008).
26. C. Vallée, T. Höhne, H. M. Prasser and T. Sühnel, *Nucl. Eng. Des.*, **238**, 637 (2008).
27. A. Tamburini, A. Cipollina, G. Micale, F. Scargiali and A. Brucato, *Ind. Eng. Chem. Res.*, **55**, 7535 (2016).
28. J. Markopoulos and E. Kontogeorgaki, *Chem. Ing. Technol.*, **65**, 839 (1993).
29. F. Scargiali, A. Busciglio, F. Grisafi and A. Brucato, *Biochem. Eng. J.*, **82**, 41 (2014).
30. Z. Driss, G. Bouzgarrou, W. Chtourou, H. Kchaou and M. S. Abid, *Eur. J. Mech. B-Fluid*, **29**, 236 (2010).
31. P. M. Armenante, C. Luo, C. C. Chou, I. Fort and J. Medek, *Chem. Eng. Sci.*, **20**, 3483 (1997).
32. A. Tamburini, A. Brucato, A. Busciglio, A. Cipollina, F. Grisafi, G. Micale, F. Scargiali and G. Vella, *Ind. Eng. Chem. Res.*, **53**, 9587 (2014).
33. R. L. Bates, P. L. Fondy and R. R. Corpstein, *I. and Ec Proc. Des. Dev.*, **2**, 310 (1963).
34. V. B. Rewatkar, K. S. M. S. Raghava Rao and J. B. Joshi, *Chem. Eng. Commun.*, **88**, 69 (1990).
35. G. Montante, K. C. Lee, A. Brucato and M. Yianneskis, *Chem. Eng. Sci.*, **56**, 3751 (2001).
36. S. Ibrahim and A. W. Nienow, *Trans. IChemE. Eng. Res. Des.*, **73**, 485 (1995).
37. K. Yapici, B. Karasozen, M. Schäfer and Y. Uludag, *Chem. Eng. Process.*, **47**, 1340 (2008).
38. L. Smit and J. During, Vortex geometry in stirred vessels, *Proceedings of the 7th European Congress on Mixing*, Belgium, Bruges **2**: 633 (1991).
39. C. Y. Ge, J. J. Wang, X. P. Gu and L. F. Feng, *Chem. Eng. Res. Des.*, **92**, 1027 (2014).
40. D. Chapple, S. M. Kresta, A. Wall and A. Afacan, *Trans. IChem. E.*, **80**, Part A, 364 (2002).
41. M. Moštěk, A. Kukuková, M. Jahoda and V. Machoň, *Chem. Pap.*, **59**, 380 (2005).
42. Cz. Kuncewicz and M. Pietrzykowski, *Chem. Eng. Sci.*, **56**, 4659 (2001).
43. F. Scargiali, A. Tamburini, G. Caputo and G. Micale, *Chem. Eng. Res. Des.*, **123**, 99 (2017).
44. A. Le Lan and H. Angelino, *Chem. Eng. Sci.*, **27**, 1969 (1972).